

1 **Elucidating loessal landslide initiation in wood- and shrub-land by hydro-mechanical**
2 **heterogeneity**

3 Ruijie Yang, Chao Ma, Xi Yang, Yan Zhang, Liqun Lyu, Xinying Wang

4 School of Soil and Water Conservation, Beijing Forestry University, Beijing 100083, PR China

5 Corresponding author: Professor Chao Ma, sanguoxumei@163.com

6 **Abstract:** Vegetation recovery on the Chinese Loess Plateau has markedly changed the hydrological and mechanical
7 controls on hillslope erosion, shifting sediment production from runoff-driven erosion to gravity-driven processes
8 such as rainfall-induced loessal landslides. Presently, few studies have clearly documented the differences in
9 landslide erosion and initiation between shrubland and woodland. We conducted field investigations, rainfall soil-
10 moisture observations, dye-tracer experiments, and soil-root tests, to examine landslide characteristics in terms of
11 geometry and volume, excess soil-water ratio, preferential-flow pathways, and failure potential in the two stands.
12 Rainfall-induced loessal landslides in the shrubland stand have shallower failure depths and smaller volumes but are
13 wider than those in the woodland stand, and they are triggered under lower contributing area-slope conditions.
14 Moreover, vertical infiltration in the woodland stand tends to be more stable and efficient, characterized by greater
15 water penetration depth and enhanced pore connectivity. The relationship between the excess soil-water ratio and
16 soil-water storage demonstrates that subsurface flow in woodland stand is triggered at relatively lower degrees of
17 saturation. This behavior is attributed to well-developed preferential-flow pathways and reduced matric suction. The
18 landscape dissection-rainfall index indicates lower landslide susceptibility on steep woodland slopes than on steep
19 shrubland slopes, consistent with the lower landslide density in woodland relative to shrubland. Overall, these
20 hydrological and mechanical contrasts indicate that woodland slopes, by combining deep root systems, stable
21 preferential-flow pathways, and strong mechanical reinforcement, support an effective subsurface flow system that
22 enhances infiltration and delays shallow saturation, thus improving slope stability. These results highlight the need
23 to reassess sediment production on the Loess Plateau by explicitly accounting for landslides rather than attributing
24 it solely to runoff-driven erosion.

25 **Keywords:** Shallow landslide; Hillslope hydrology; Landscape dissection-rainfall index

26 **1 Introduction**

27 The Chinese Loess Plateau is one of the most erosive landscapes in the world (Fu et al., 2016; Borrelli et al.,
28 2020; Bai et al., 2024). Since 1980, ecological rehabilitation has significantly improved regional vegetation cover
29 and structure, with vegetation cover now reaching approximately 60% (Feng et al., 2016; Deng et al., 2022; Liao et
30 al., 2025). Restored vegetation, optimized plant community structure, and surface litter accumulation have enhanced
31 water storage capacity and slope stability (Yan et al., 2024; Liu et al., 2025). Since 2010, the region has experienced
32 several rainstorms that are unprecedented in the historical record, as exemplified by storms in 2013, 2017, and 2025
33 (Tang et al., 2020; Deng et al., 2022; Yang et al., 2023; Hao et al., 2024). Subsequent studies have reported a shift
34 in the dominant erosion process from dispersed runoff erosion to gravitational mass movements (Yang et al., 2024;
35 Du et al., 2025). These findings sufficiently indicate that vegetation recovery on Chinese Loess Plateau alters the
36 dominant sediment-producing processes and soil-erosion patterns.

37 Vegetation recovery can enhance ecosystem functioning and alter the rainwater infiltration pathways (Gu et al.,
38 2019; Wang et al., 2022; Guan et al., 2024). Increases in surface cover and root penetration significantly enhance
39 rainfall infiltration and promote greater spatial heterogeneity, non-uniform infiltration patterns, and preferential-flow
40 pathways (Li et al., 2007; Zhao et al., 2022). Preferential flow often serves as a primary pathway for rainfall
41 infiltration and can bypass soil-matrix pores to reach deeper soil layers (Bachmair et al., 2012; Franklin et al., 2021).

42 Preferential flow intensity and morphology vary markedly among vegetation types. Woodland slopes are
43 characterized by deep, continuous macropore channels, predominantly vertical preferential flow, rapid infiltration,
44 and greater deep-soil water storage (Niu et al., 2023; Cai et al., 2024; Zhang et al., 2025). Shrubland slopes exhibit
45 predominantly lateral and diffuse subsurface flow with weak vertical components, thereby retaining much of the
46 infiltrating water in shallow soil layers (Wang et al., 2020; An et al., 2022; Liang et al., 2023; Zhang et al., 2024).
47 Herbaceous slopes rely mainly on surface cracks and earthworm burrows to route water, and therefore preferential
48 flow channels are sparse and discontinuous (Wen et al., 2020; Niu et al., 2023; Li et al., 2025). Vegetation recovery
49 has significantly restructured the soil bio-pore system through root penetration, thereby facilitating the development
50 of preferential-flow pathways and making infiltration regimes more heterogeneous (Zhao et al., 2022; Guan et al.,
51 2024). However, preferential-flow infiltration on steep slopes, particularly at landslide sites with different vegetation
52 types, has not been adequately investigated. During heavy storms, preferential flow can regulate spatiotemporal
53 subsurface water dynamics and act as a biologically mediated control on slope stability.

54 Root morphology and spatial configuration influence rainwater infiltration pathways and soil-moisture
55 redistribution (Fan et al., 2020; Li et al., 2023). On the Chinese Loess Plateau, two predominant vegetation types are
56 recognized: woodlands dominated by *Robinia pseudoacacia* and *Pinus tabulaeformis*, and shrublands dominated by
57 *Rosa xanthina* and *Hippophae rhamnoides*. Woodland trees typically develop deeply penetrating root systems,
58 forming continuous macropore networks and vertical preferential-flow pathways (Zhao et al., 2022; Cai et al., 2024;
59 Wang and Zhang, 2024). These structures facilitate rapid rainfall infiltration into deep soil layers, enhance subsurface
60 moisture retention, delay surface saturation, and reduce surface runoff (Souza et al., 2023; Cai et al., 2024; Hu et al.,
61 2025). In contrast, shrubs develop a dense, fibrous root matrix that promotes mesopores and capillaries formation,
62 thereby accelerating the formation of subsurface saturation zones and limiting vertical percolation (Laycock et al.,
63 1967; Souza et al., 2023; Xiao et al., 2024; Yamase et al., 2024). Therefore, plant roots can control preferential-flow
64 patterns and alter hillslope hydrology. However, few studies have examined how the hydrological effects of mature
65 vegetation influence landslides on the Chinese Loess Plateau.

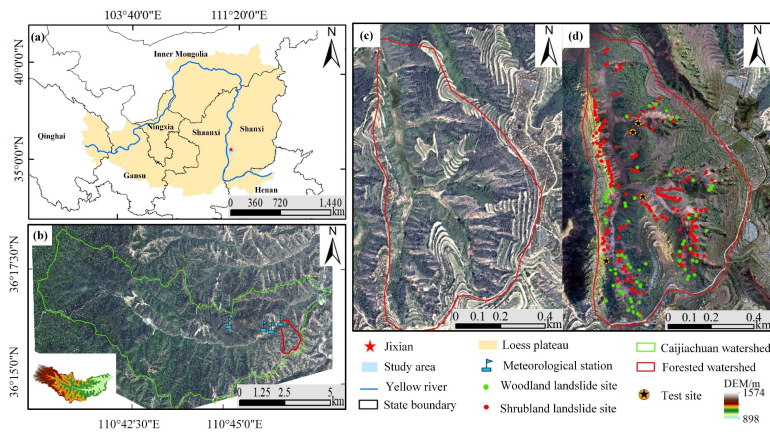
66 To examine the hydrological and mechanical heterogeneity in mature woodland and shrubland stands on steep
67 slopes and its implications for slope stability, we first analyze landslide geometry and landscape dissection for slides
68 triggered by a low-intensity storm from 3 to 6 October 2021. Then, we assess hydrological heterogeneity in mature
69 woodland and shrubland using soil-moisture observations, excess soil-water ratios across different soil-water storage
70 levels, and preferential-flow pathway identification. Mechanical heterogeneity is characterized by soil and root
71 strength parameters, the soil water characteristic curve (SWCC), and the hydraulic conductivity function (HCF).
72 Finally, we evaluate slope failure potential in relation to landslide density in the two stands. This study mainly
73 addresses the role of vegetation in modulating slope stability by analyzing real landslide cases. Our findings highlight
74 the dual role of vegetation in mitigating landslide erosion and provide new insights into its nuanced effects on
75 hillslope stability.

76 2. Research background

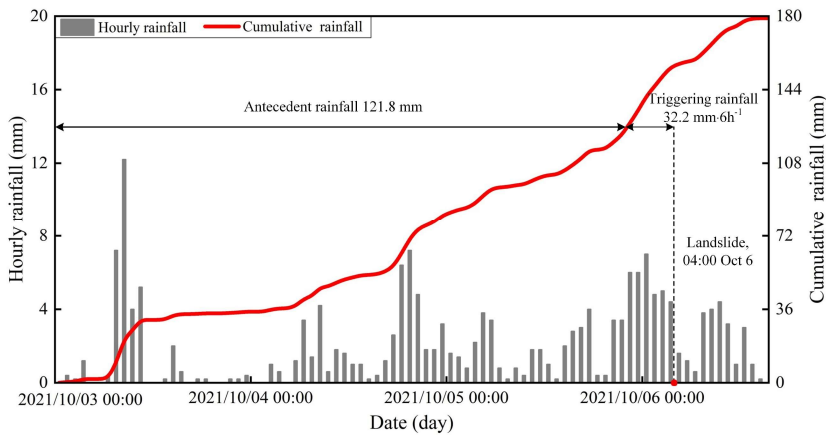
77 2.1 Study area

78 The study area lies in a forested catchment on the southeastern Loess Plateau in China (Fig. 1a). It is located in
79 the downstream reach of the Caijiachuan watershed in Jixian County, Shanxi Province (Fig. 1b). The soil has an
80 unconsolidated, porous structure. On steep slopes, woodland is dominated by *Robinia pseudoacacia* and shrubland
81 by *Rosa xanthina*. Since the farmland reforestation policy was implemented in 1980, forest cover has recovered to
82 about 70%. During 1990–1995 and 1999–2002, the Mountain Improvement Technology Training Project enhanced
83 forest regeneration. Currently, the local soil and water conservation measures serve as a benchmark within the Loess

84 Plateau region. The area has four distinctive seasons and a cold semi-arid climate . The annual precipitation is
 85 approximately 579.1 mm, and the mean annual temperature is 9.9°C. Most rain events occurs from June to September,
 86 accounting for more than 70% of the annual precipitation. Prior to the 2021 event, a short-duration storm on 25–26
 87 August 2003 triggered 18 landslides, with antecedent precipitation of 71.7 mm over 18 hours and an intense 3 h
 88 rainfall of 24.4 mm (Wang et al., 2024). In contrast, the 2021 rainfall event was a low-intensity storm with prolonged
 89 antecedent precipitation of 121.8 mm over 72 hours and a 6 h peak rainfall of 32.2 mm (Fig. 2). After the storm,
 90 post-storm documentation mainly focused on differences in landslide numbers, densities, slope aspects, and
 91 morphological metrics (Tang et al., 2023), while giving little attention to the hydrological and mechanical conditions
 92 of landslides in the two forested land types.



93
 94 **Figure 1.** Geographical setting of the study area, with the (a) location of Caijiachuan watershed in the Loess Plateau,
 95 China, (b) the forested catchment and meteorological stations in downstream reach of Caijiachuan watershed, (c)
 96 0.15 m resolution orthoimage on 12 October 2019, and (d) 0.10 m resolution orthoimage on 14 October 2021
 97 showing the sites for soil-moisture observations and dye-tracer experiments.



98
 99 **Figure 2.** Hourly and cumulative rainfall from 3 to 6 October 2021.

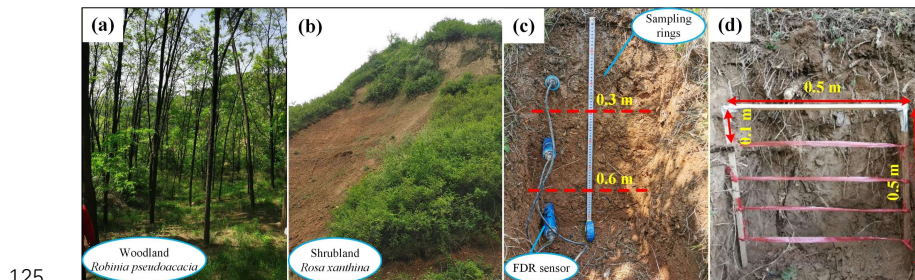
100 3 Materials and methods

101 3.1 Landslide information interpretation

102 To obtain landslide inventories for the woodland and shrubland, we acquired high-resolution orthoimages and
103 digital elevation models (DEMs) using an unmanned aerial vehicle (UAV; DJI Inspire 2). Two systematic UAV
104 flights with consistent flight and image overlap settings were conducted on 12 October 2019 (Fig. 1c) and 14 October
105 2021 (Fig. 1d). Pix4Dmapper (version 4.6, Pix4D SA, Switzerland) was used to generate ortho-mosaics and DEMs.
106 These DEMs have spatial resolutions of 0.15 m and 0.10 m, respectively, thereby supporting accurate landslide
107 mapping. The landslide depths in the woodland and shrubland were measured during field investigations. Landslide
108 point and areal densities are calculated by dividing the total number of landslides and the total scar area by the
109 woodland and shrubland areas, respectively. The lateral extent of each landslide is the sum of the sidewall and head
110 scarp areas. The unit upslope contributing area is the ratio of the total contributing area to the scar width. Slope
111 gradients and associated unit contributing areas are computed from the DEM generated on 14 October 2021.

112 3.2 Rainfall, soil-moisture monitoring and sample collection

113 In the study area, the woodland has an open structure due to sparse-to-moderate tree density and high canopy
114 height (Fig. 3a), whereas the shrubland has a closed structure because of high density and low canopy height (Fig.
115 3b). Each study site is dominated by single woody species, with *Robinia pseudoacacia* in the woodland and *Rosa*
116 *xanthina* in the shrubland. Both land types have a well-developed herbaceous layer. To investigate the hillslope
117 hydrology, we used frequency-domain reflectometry (FDR) soil-moisture sensors installed at depths of 30, 60, and
118 90 cm to record volumetric water content from May to August 2023 (Fig. 3c). A meteorological station at
119 Caijiachuan Forest Station is approximately 2 kilometers to the northwest of the study area. During soil-moisture
120 sensor installation, we collected undisturbed soil samples near the FDR sensor locations. Bulk density, porosity,
121 effective cohesion, internal friction angle, and unsaturated hydraulic properties were determined using an electronic
122 balance, an oven, a GDS triaxial apparatus, and transient release and imbibition tests (Lu and Godt, 2013). Plant
123 roots were collected to determine depth-dependent root distribution (Fig. 3d), root diameter, root area ratio, and
124 tensile strength (Nimmo et al., 2009).



125 **Figure 3.** Soil moisture monitoring and soil and root sampling. (a) Open woodland dominated by *Robinia*
126 *pseudoacacia*. (b) Close-structure shrubland dominated by *Rosa xanthina*. (c) Trench wall showing soil sampling
127 and FDR sensor installation. (d) In situ root counting and sampling at 0.1 m depth intervals.

129 3.3 Excessive soil water due to preferential flow

130 Previous studies of preferential flow on the Loess Plateau have shown that continuous channels in woodland
131 enhance deep soil water storage, whereas lateral and dispersed channels in shrubland keep water in shallow soil
132 layers (Wang et al., 2019; An et al., 2022). Therefore, differences in preferential-flow pathways can result in distinct
133 soil-moisture responses during the same rainfall event. In this study, we first characterized preferential-flow

删除了: on

135 pathways using dye tracer experiments and then examined soil-moisture responses using observed soil-moisture data.
 136 Dye tracer experiments were conducted on vegetated slopes near the soil-moisture monitoring sites to examine
 137 the preferential flow pathways (Fig. 1d). The slope angles were 35.8° at the woodland site and 38.2° at the
 138 shrubland site. An electric sprayer was used to spray a $4 \text{ g}\cdot\text{L}^{-1}$ brilliant blue solution onto a $100 \text{ cm} \times 100 \text{ cm}$ plot
 139 (Figs. 4a and 4b). After spraying the solution, the plot was immediately covered with a rainproof cloth to minimize
 140 evaporation. After 24 h, a 5 cm-wide margin of soil was removed from the plot edges, and the core area was
 141 excavated to obtain 10 vertical and 5 horizontal profiles. Excavation grids were established at 0.1 m intervals in both
 142 the longitudinal and transverse directions (Figs. 4c and 4d). Profile images were captured with a digital camera at a
 143 fixed distance and in a parallel orientation, and subsequently processed using Adobe Photoshop (version 2021;
 144 Adobe Inc., USA) and Image-Pro Plus (version 6.0; Media Cybernetics, USA). The proportion of flow marked by
 145 the dye is:

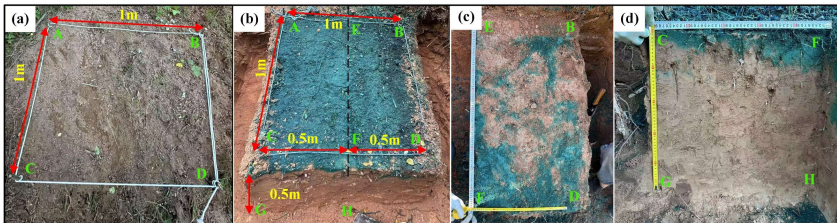
$$SAR = \frac{a_j}{A_j} \quad (1)$$

147 where SAR is the stained-area ratio for the soil profile, j is soil depth (cm), a is the number of stained pixels at
 148 depth j , and A is the total number of pixels along the image width at depth j .

149 The soil-moisture response index describes excess soil water in response to a given rainfall input:

$$R_C = \frac{R_{max} - (R + R_0)}{R + R_0} \quad (2)$$

151 where R_C is the excess soil-water ratio in response to a given rainfall event, R_{max} is the maximum total soil-water
 152 storage during the rainfall episode (mm), R is the cumulative rainfall during the episode (mm), and R_0 is the initial
 153 total soil-water storage before the rainfall episode (mm). Positive or negative values of R_C indicate whether the
 154 increase in soil-water storage exceeds or falls below the rainfall input. In addition, R_C reflects the preferential-flow
 155 component aligned with slope orientation or gravity. As soil moisture typically lags rainfall, we follow the method
 156 proposed by Lu et al. (Lu et al., 2024), which defines rainfall episodes using soil depth and in situ saturated hydraulic
 157 conductivity measurements. Therefore, the R_C values under different $R + R_0$ conditions, together with the
 158 preferential-flow pathways, can reflect heterogeneity in soil-water movement in the woodland and shrubland.



159
 160 **Figure 4.** Dye tracer experiments and preferential flow pathways examination. (a) Experimental plot after vegetation
 161 removal. (b) Experimental plot after 24 h of brilliant blue solution spraying. (c) Dye-stained profile parallel to the
 162 slope surface. (d) Dye-stained profile along the gravity direction. Capital letters denote corresponding points shared
 163 across Fig. 4a-d.

164 3.4 Slope resistance to failure probability at given rainfall input

165 Hillslope resistance to failure at a given rainfall input depends on the topography and the physical, strength,
 166 and hydraulic properties of soil mass. A widely used combination of the infinite-slope stability model and a
 167 hydrological model yield an expression for the critical drainage area per unit contour length (Montgomery and
 168 Dietrich, 1994):

删除了:
 删除了: -

171
$$a_{cr} = \frac{zK\sin\theta\cos\theta}{R_t} \left[\frac{C'+C_r}{\rho_w g z \cos^2\theta \tan\varphi} + \frac{\rho_s}{\rho_w} \left(1 - \frac{\tan\theta}{\tan\varphi} \right) \right] \quad (3)$$

172 where a_{cr} is the critical drainage area per unit contour length ($\text{m}^2\cdot\text{m}^{-1}$), R_t is the triggering rainfall rate ($\text{m}\cdot\text{d}^{-1}$),
 173 K is the saturated hydraulic conductivity ($\text{m}\cdot\text{d}^{-1}$), θ is the slope angle ($^\circ$), C' and C_r are the effective soil
 174 cohesion and the root-induced cohesion (kPa), ρ_s and ρ_w are the unit weights of soil and water ($\text{KN}\cdot\text{m}^{-3}$), z is
 175 the landslide depth (m), and φ is the effective internal friction angle ($^\circ$).

176 The left-hand side of Eq. (3) represents the topographic condition of a given landslide or a site susceptible to
 177 slope failure (Montgomery et al., 2000). Moving R to the left-hand side yields the right-hand side of Eq. (4) in an
 178 integrated form involving only soil mass parameters:

179
$$a_{cr} \times R_t = \frac{K \tan\theta (C'+C_r)}{\rho_w g \tan\varphi} + zK\sin\theta\cos\theta \frac{\rho_s}{\rho_w} \left(1 - \frac{\tan\theta}{\tan\varphi} \right) \quad (4)$$

180 The physical meaning of $a_{cr} \times R_t$ is that hillslope resistance to failure under site-specific topographic conditions and
 181 a given rainfall input strongly depends on soil physical properties. For the rain-induced loessal landslides in the
 182 study area, the strength and hydraulic properties of the landslide mass in woodland and shrubland may lead to
 183 different $a_{cr} \times R_t$ levels, so that landslide density (or number) differs between woodland and shrubland. Therefore,
 184 we focus on $a_{cr} \times R_t$ from the right-hand side of Eq. (4) to elucidate the initiation of loessal landslides in two forested
 185 land types.

186 **4 Results**

187 **4.1 Landslides in the two lands**

188 To compare the landslide point and areal densities between the two stands, we calculated landslide counts and
 189 areas and divided them by the total steep-terrain area in each stand. This approach excluded non-susceptible terrain
 190 from the analysis. The spatial distribution and morphology of landslides in woodland and shrubland exhibited clear
 191 patterns. Specifically, the statistical results showed that landslide point density in shrubland was 1.56 times that in
 192 woodland, whereas landslide areal density was only 0.48 times that in woodland (Figs. 5a and 5b). Furthermore, the
 193 average landslide width in shrubland was 1.49 times that in woodland. Generally, trees in woodlands have deep root
 194 systems that provide stronger anchoring and can mobilize deeper soil layers, thereby modifying the failure depth
 195 and geometry of shallow landslides (Schwarz et al., 2010; Masi et al., 2023; Dibiagio et al., 2024). The average
 196 landslide depth in woodland was 1.82 times that in shrubland, while the average lateral extent was 1.61 times that in
 197 shrubland. However, the average width of landslides in woodland was only 0.67 times that in shrubland. Overall,
 198 the total landslide volume in woodland was 1.16 times that in shrubland, indicating that landslides in woodland tend
 199 to be larger (Figs. 5c and 5d).

200 When landslides are considered alongside other landscape-dissection agents such as rills and gullies, their
 201 spatial locations depend on two controls. One is spatial competition between the slope-dependent term $S = \tan\theta$
 202 ($\text{m}\cdot\text{m}^{-1}$) and the area-dependent term A ($\text{m}^2\cdot\text{m}^{-1}$); the other is exceedance of the A - S topographic threshold
 203 (Montgomery and Dietrich, 1994). As highlighted in Sect. 3.4, variations in $a_{cr} \times R_t$ arise from the interplay of
 204 topography, failure depth, soil strength, plant root reinforcement, and hydraulic conductivity. To evaluate these
 205 controls on landslides, we compared the upslope contributing area (A) and slope gradient (S) between the two land
 206 types.

207 Field investigations reveal that most landslides in the study area occur in concave topographic positions.
 208 Statistical analysis indicates that, on average, woodland sites have a significantly larger upslope contributing area
 209 ($124 \text{ m}^2 \text{ m}^{-1}$) and steeper slopes (48°) than shrubland sites. These values are consistent with expectations from the
 210 A - S threshold framework (Fig. 6a). Fitting regression lines to the bin-averaged dataset further demonstrates that

删除了: soil thickness

删除了: $a_{cr} \times R_t$

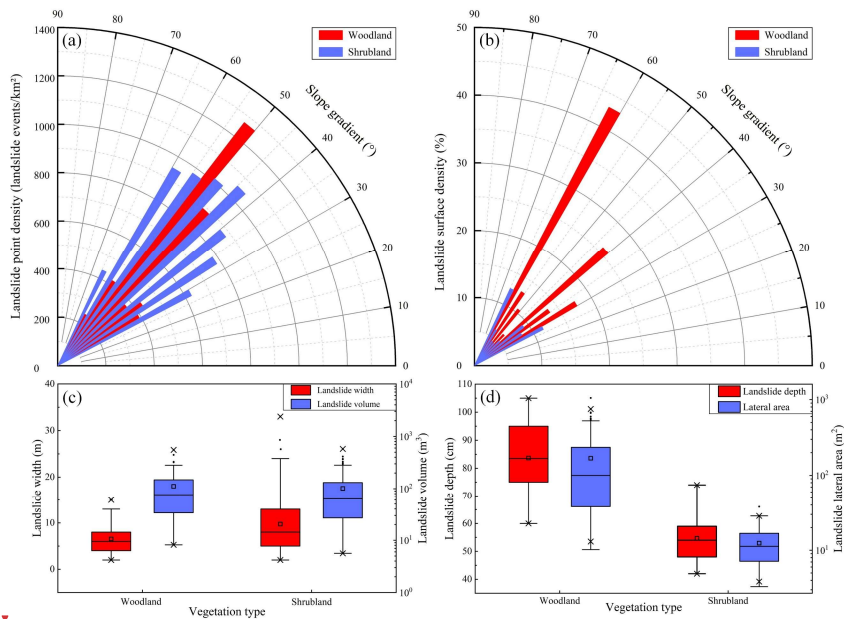
删除了: $a_{cr} \times R_t$

删除了: $a_{cr} \times R_t$

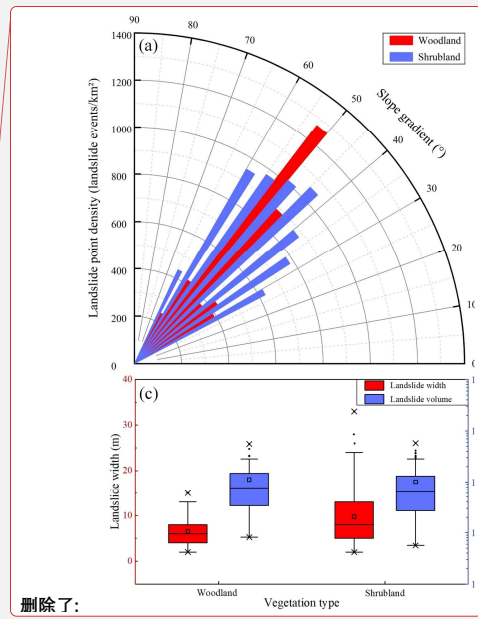
删除了: $a_{cr} \times R_t$ arise

设置了格式: 非上标/下标

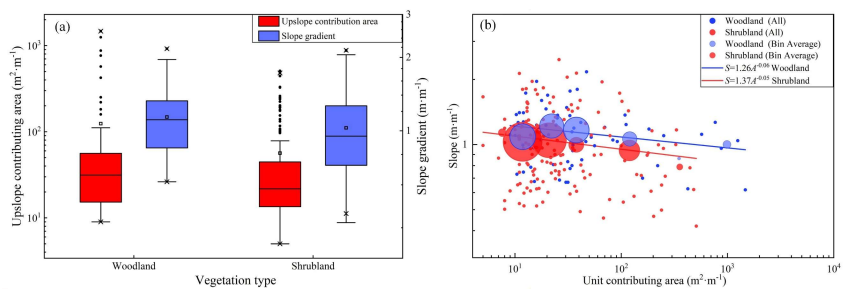
216 landslides in woodland generally require either a larger upslope contributing area or a steeper slope gradient for
 217 initiation (Fig. 6b). The $A-S$ relationship shows that, at similar slope gradients, landslides in woodland require larger
 218 upslope contributing areas than those in shrubland. This suggests that, compared with landslides in shrubland, those
 219 in woodland may require higher rainfall-intensity thresholds, steeper slopes, or both, for initiation. Consistent with
 220 this, shrubland shows a higher landslide point density than woodland (1.56 times; Fig. 5a).



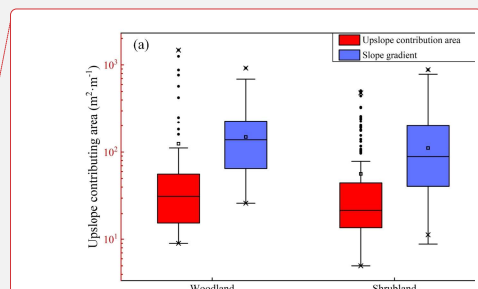
221
 222 **Figure 5.** Landslide characteristics in woodland and shrubland. (a) point density by slope-gradient class; (b) areal
 223 density by slope-gradient class; (c) landslide width and volume, and (d) landslide depth and lateral area. The three
 224 horizontal-lines of box show decreasing order of 75th quantile (Q_3), median (Q_2), and 25th quantile (Q_1). The box
 225 length is the interquartile range ($IQR=Q_3-Q_1$). The small square is the average value. The cross symbols denote the
 226 1st and 99th percentiles. The upper and lower limit of whiskers are $Q_3+1.5IQR$ and $Q_1-1.5IQR$, respectively. The
 227 whiskers extend to the most extreme values within these limits; mild outliers are shown as black dots.



删除了: landslide depth and lateral area
 删除了:
 删除了: landslide width and volume



228
 229 **Figure 6.** Upslope contributing area and slope gradient condition. (a) upslope contributing area and mean slope as a
 230 function of slope aspect; (b) upslope contributing area vs. mean slope gradient above the landslide area. The



删除了: -

237 definition of the boxplots is given in the caption of Fig. 5. Circles indicate mean slopes, with radius proportional to
 238 the number of landslides. A power-law regression is fitted to the bin-averaged data.

239 4.2 Soil Hydrological properties

240 4.2.1 SWCC and HCF curves

241 Mean landslide depths in woodland and shrubland are 0.84 m and 0.55 m, respectively (Fig. 5d). Soil-moisture
 242 monitoring and soil sampling were conducted at three depth intervals (0–30, 30–60, and 60–90 cm), as described in
 243 Sect. 3.2. Because observed landslide depths in woodland were mostly within 60–90 cm, this layer was taken as the
 244 representative sliding layer for woodland. Likewise, because observed landslide depths in shrubland were mostly
 245 within 30–60 cm, this layer was taken as the representative sliding layer for shrubland. Loess slopes generally remain
 246 unsaturated during natural rainfall infiltration and drainage (Lan et al., 2021; Wei et al., 2022). Therefore, we used
 247 the SWCC and HCF to analyze unsaturated hydro-mechanical differences between sliding-layer soils in woodland
 248 and shrubland.

249 Table 1 lists the sliding-layer soils parameters obtained through Hydrus-1D inversion. Based on these
 250 parameters, the SWCC and HCF were plotted for the woodland and shrubland sliding-layer soils (Fig. 7). The results
 251 indicate that the pore-size distribution parameter and saturated hydraulic conductivity are significantly higher for
 252 woodland soils than for shrubland soils. This contrast is evident in both drying and wetting processes. This suggests
 253 that the pore system in woodland soils is dominated by larger pores, which enhance water movement. This pore
 254 structure facilitates rainfall infiltration into the soil. In contrast, shrubland soils contain more micropores that retain
 255 more water. This is reflected in a 3.1% higher residual water content in shrubland soils than in woodland soils.
 256 During the drying test, the air-entry pressures of woodland and shrubland soils are nearly identical. However, during
 257 the wetting process, the air-entry pressure in woodland soils is 0.05 kPa lower than in shrubland soils. This indicates
 258 that larger pores in woodland soils begin to drain and fill with air at lower matric suction. This promotes air-water
 259 exchange and moisture release, making it less likely for the soil to reach or maintain a high degree of saturation for
 260 extended periods. Therefore, under the same rainfall conditions, shrubland soils have weaker moisture-buffering
 261 capacity than woodland soils, making the soil more prone to becoming highly saturated. This reduces the effective
 262 stress and shear strength of shrubland soils, ultimately reducing slope stability.

263 During the drying and wetting processes, the difference in saturated water content in shrubland sliding-layer
 264 soil (0.101) is approximately 14.43 times that in woodland sliding-layer soil (0.007). This indicates that the pore
 265 structure in shrubland sliding-layer soil is less stable than in woodland sliding-layer soil. Under extreme drying-
 266 wetting conditions, some pores tend to collapse or rearrange, making it difficult for the soil to maintain its original
 267 pore configuration. The resulting changes in pore structure disrupt water flow paths in shrubland sliding-layer soil,
 268 reducing permeability, weakening water flow, and slowing drainage. These findings are consistent with the stronger
 269 hysteresis observed in the SWCC of shrubland sliding-layer soil compared with that of woodland sliding-layer soil
 270 (Figs. 7a and 7b). They further confirm that woodland sliding-layer soil has a greater capacity for moisture
 271 redistribution.

272 **Table 1.** Parameters describing the soil water characteristic curve (SWCC) and the hydraulic conductivity function
 273 (HCF) for the sliding-layer soils used in Hydrus 1D

Parameters	Definition	Woodland	Shrubland
θ_s^d	Saturated water content	0.500	0.480
θ_s^w		0.493	0.379
θ_r	Residual water content	0.055	0.086
n^d	The pore size distribution parameter	1.58	2.19
n^w		1.69	1.88

删除了: Extensive research has examined saturated hydraulic conductivity and microstructural properties of loess (Xu et al., 2021; Li et al., 2023). Given that loess on hillslopes largely remains unsaturated during natural rainfall infiltration and drainage

删除了: , evaluating unsaturated hydro-mechanical differences using SWCCs and HCFs is important. Therefore, this approach enables comparison among key parameters—hydraulic conductivity, matric suction, suction stress, and microstructural properties.

删除了:

删除了: and

删除了: from

σ^d (KPa ⁻¹)	The inverse of the air entry pressure head	5.461×10^{-3}	6.294×10^{-3}
σ^w (KPa ⁻¹)		0.646	0.596
K_s^d (cm·s ⁻¹)	Saturated hydraulic conductivity	2.3×10^{-5}	5.4×10^{-6}
K_s^w (cm·s ⁻¹)		7.1×10^{-2}	5.0×10^{-3}

Notes: Superscripts "d" and "w" denote the drying and wetting processes, respectively.

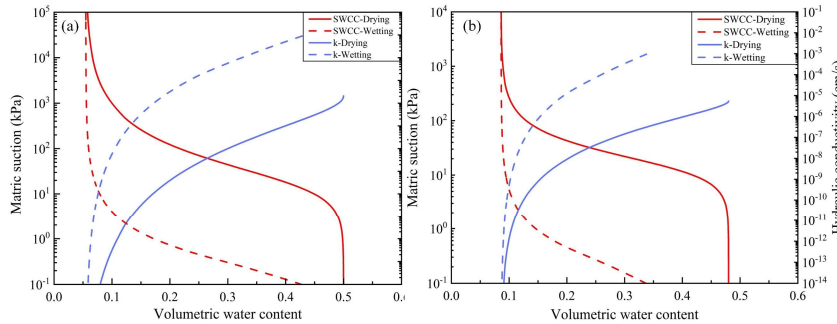
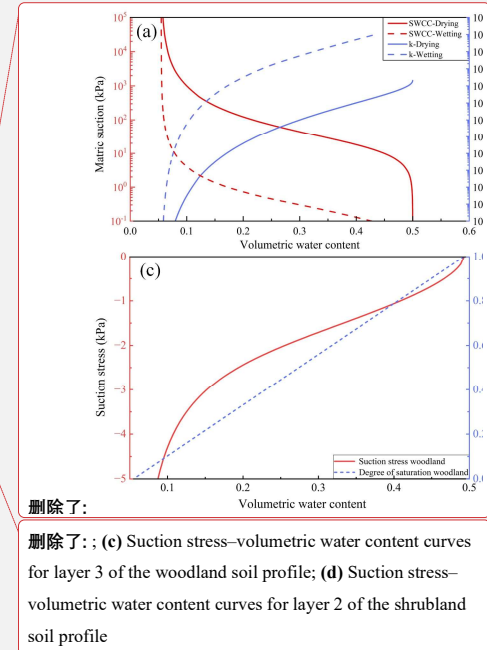


Figure 7. Differences in the hydromechanical properties of the sliding-layer soils. **(a)** SWCC for layer 3 of the woodland soil profile; **(b)** SWCC for layer 2 of the shrubland soil profile.

4.2.2 Dye tracer experiments

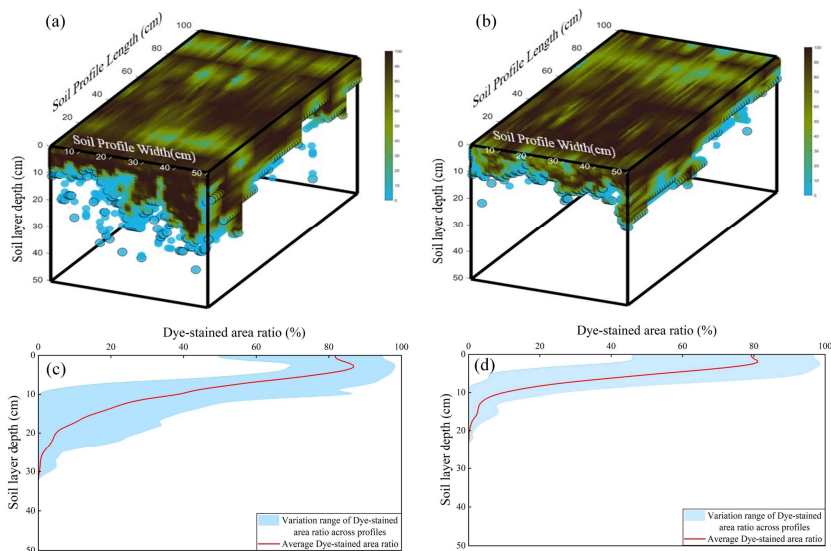
Dye-tracer experiments directly visualize the flow pathways of water infiltration in woodland and shrubland soils. Under the same applied water volume and infiltration area, the stained soil volume in woodland soils is markedly larger than that in shrubland soils. Three-dimensional visualizations reveal that stained pathways in woodland soils form thick bands with numerous vertically continuous columnar channels. Hydraulic connectivity is high, and water infiltrates to greater depths. Stained bands in shrubland soils are shallow, and vertical, filament-like channels are nearly absent. In addition, the depth-dependent pattern of dye-stained area ratios in the shrubland profile further confirms that vertical infiltration is restricted to relatively shallow depths. Differences in the volume, depth, and morphology of the stained pathways indicate that infiltration in woodland soils no longer follows uniform matrix-flow conditions. This is also evident in the dye-stained areas of vertical profiles. Woodland profiles show large, continuous color patches, whereas shrubland profiles mainly show fragmented spots concentrated in shallow soil. This pattern suggests that deeper shrubland soils are denser and have lower pore connectivity.

Overall, woodland soils more readily develop a stable, efficient vertical percolation system with greater infiltration depth and stronger connectivity. This promotes deep water storage and redistribution. In contrast, insufficient pore connectivity in shrubland soils causes water to remain in shallow layers, prolonging surface wetness and slowing pore-water pressure recovery. Under intense rainfall, this condition favors saturation buildup and thus increases the likelihood of landslide initiation. This flow pattern is consistent with the SWCC- and HCF-inferred differences in soil hydraulic behavior and provides direct, pathway-scale evidence of flow pathways, which cannot be resolved from the curve-derived hydraulic parameters alone.

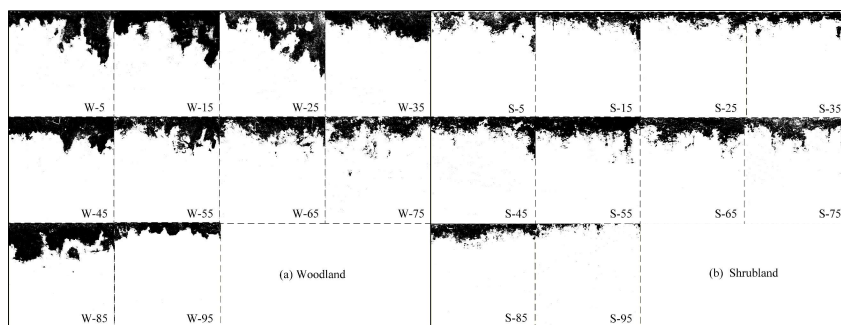


删除了:

删除了: **(c)** Suction stress–volumetric water content curves for layer 3 of the woodland soil profile; **(d)** Suction stress–volumetric water content curves for layer 2 of the shrubland soil profile



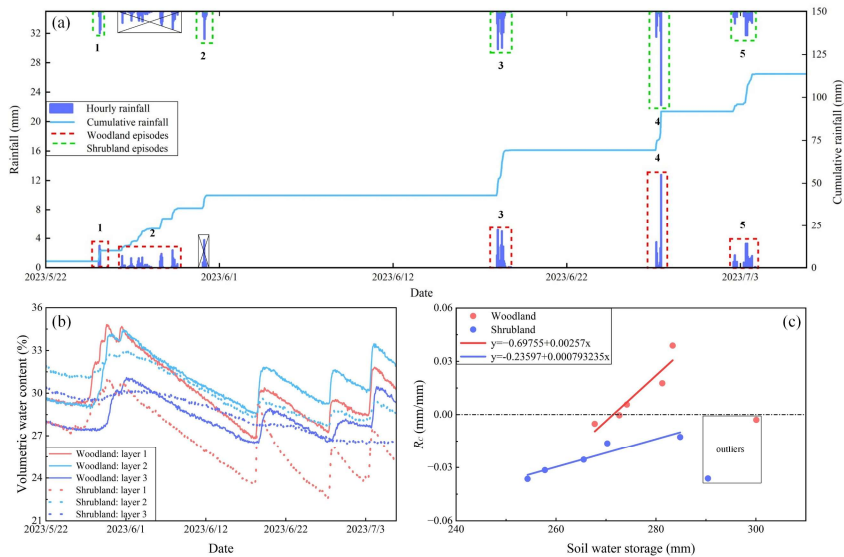
317
 318 **Figure 8.** Morphological characteristics of dye-stained flow paths in woodland and shrubland soils. **(a)** Three-
 319 dimensional visualization of stained zones in woodland; **(b)** Three-dimensional visualization of stained zones in
 320 shrubland; **(c)** Dye-stained area ratio vs. soil depth in woodland; **(d)** Dye-stained area ratio vs. soil depth in shrubland.



321
 322 **Figure 9.** Schematic dye-stained vertical soil profiles at different hillslope positions. **(a)** Woodland profile; **(b)**
 323 Shrubland profile. Numbers from 0 to 100 denote relative slope positions, with lower values indicating locations
 324 near the slope base.

325 4.3 Slope hydrological characteristics

326 To characterize how woodland and shrubland soils respond to rainfall, we group rainfall events into distinct
 327 episodes based on soil depth and in rain saturated hydraulic conductivity (Fig. 10a). Using these episodes as the
 328 basic analytical units, we then assess the intensity of slope-surface responses and the associated water distribution.
 329 This approach overcomes the limitations of using rainfall statistics alone. It explicitly addresses the slope's dynamic
 330 absorption-response behavior and shifts the focus from single-storm triggering to a more comprehensive assessment
 331 of cumulative rainfall-response lags.



332
 333 **Figure 10.** Analysis of rainfall, soil moisture, and their coupling from 22 May to 7 July 2023. **(a)** Classification of
 334 rainfall episodes by vegetation type; **(b)** Temporal variation in volumetric soil water content for woodland and
 335 shrubland; **(c)** Coupling between rainfall input and soil-moisture response for woodland and shrubland.

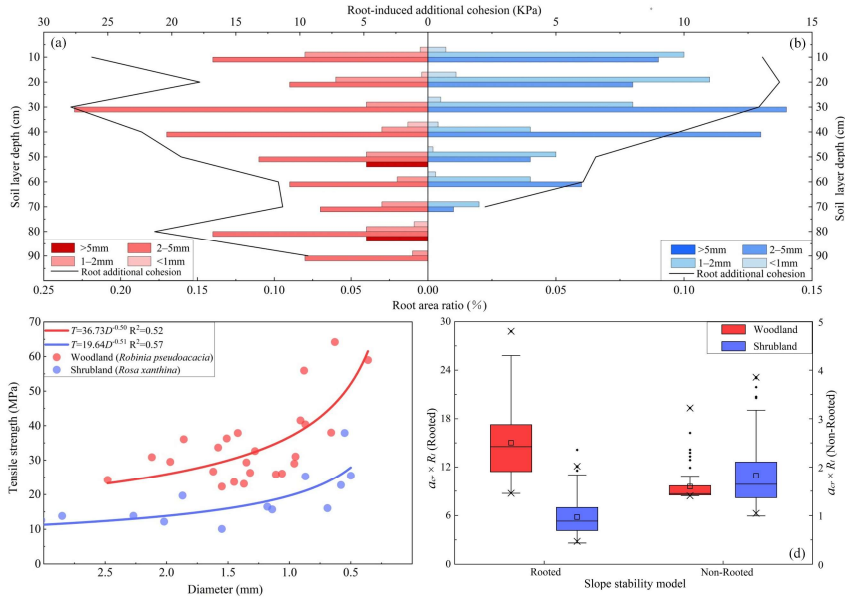
336 From 22 May to 7 July 2023, volumetric water content indicates that shrubland soils beneath the sliding layer
 337 (layer 3) are insensitive to rainfall and show only small variations in water content (Fig. 10b). This is consistent with
 338 the findings in Sect. 4.2. In shrubland, most water remains near the surface, and infiltration capacity is low. To
 339 characterize the rainfall-soil-water coupling process, we introduce the index R_c , which quantifies how efficiently
 340 rainfall is converted into soil-water storage (Fig. 10c). A steeper slope in the regression of R_c versus soil water
 341 storage indicates a stronger soil-moisture response to rainfall.

342 In woodland, R_c values are generally positive, indicating that increases in soil-water content often exceed local
 343 rainfall input. Woodland soils have better-developed preferential flow paths than shrubland soils. This suggests that
 344 the observed excess arises because water infiltrating into upslope soils moves downslope as subsurface flow. This
 345 interpretation is consistent with the dye-tracer experiments. In woodland, foot-slope profiles show greater staining
 346 depths than upslope profiles (Fig. 8a). By contrast, early shallow saturation in shrubland diverts part of the rainfall
 347 input into overland flow, reducing conversion efficiency and yielding mostly negative R_c values. Overall, high R_c
 348 values in woodland reflect a strong hydrological response to rainfall and a greater capacity to buffer soil moisture.
 349 In shrubland, a pronounced response lag and low conversion efficiency lead to negative R_c values. These patterns
 350 are consistent with the earlier mechanism-based interpretation.

351 4.4 Effects of vegetation roots on hillslope stability

352 Root spatial distribution and mechanical properties differ markedly between woodland and shrubland soils
 353 (Figs. 11a, 11b, and 11c). Field measurements indicate that maximum rooting depths in *Robinia pseudoacacia* and
 354 *Rosa xanthina* are close to their respective mean landslide depths, at 0.84 m in *Robinia pseudoacacia* and 0.54 m in
 355 *Rosa xanthina*. This consistency indicates a close relationship between root distribution and landslide depth.
 356 Compared with *Rosa xanthina*, roots in *Robinia pseudoacacia* mobilize greater root-induced cohesion at a given

357 root diameter and exhibit a larger specific root area ratio (*RAR*). These roots therefore create a more extensive root-
 358 soil contact interface and form a mechanically stronger root-soil composite.



359
 360 **Figure 11.** Mechanical indices of slope stability in woodland and shrubland. (a) Root area ratio and root-induced
 361 cohesion in woodland (*Robinia pseudoacacia*); (b) Root area ratio and root-induced cohesion in shrubland (*Rosa*
 362 *xanthina*); (c) Relationship between root tensile strength and diameter; (d) Slope-stability models for woodland and
 363 shrubland. The definitions of the boxplots is given in the caption of Fig. 5.

364 Using the parameters in Table 2, we constructed a slope stability model to evaluate slope resistance to failure
 365 under specified topographic conditions and rainfall inputs. When root-induced cohesion is ignored, mean $a_{cr} \times R_t$
 366 values in woodland and shrubland are similar, indicating that slope stability differs little between them. When root
 367 effects are included, slope stability increases markedly. In woodland, the $a_{cr} \times R_t$ value rises to 15.02, approximately
 368 338% higher than in shrubland (Fig. 11d). These results indicate that woodland roots contribute much more to slope
 369 stability than roots in shrubland. Woodland roots substantially increase the critical rainfall and topographic
 370 thresholds for landslide initiation and confirm the key role of roots in strengthening slopes and resisting landslide-
 371 triggering factors.

372 **Table 2** Parameters describing the slope stability model

Parameters	Definition	Woodland	Shrubland
ρ_s (kg m^{-3})	Dry soil density	1.37	1.41
θ ($^\circ$)	Slope gradient	31.71–65.27	22.78–67.96
C' (kPa)	Effective soil cohesion	5.97	7.35
C_r (kPa)	Root-induced cohesion	18.59	10.36
φ ($^\circ$)	Effective friction angle	18.67	14.50
z (m)	Landslide depth	0.84	0.54
K (mm h^{-1})	Hydraulic conductivity	2.10	0.94

删除了: $a_{cr} \times R_t$
 设置了格式: 非上标/下标

374 **5 Discussion**

375 Long-term vegetation restoration policies may result in the dominant soil erosion process shift from traditional
376 wind and water erosion to landslides (Deng et al., 2022; Yang et al., 2024; Du et al., 2025; Liao et al., 2025).
377 Ecological restoration forests not only increase surface cover, but the recovered vegetation extends their root systems
378 into potential sliding layers, thereby substantially altering slope hydrological processes and mechanical properties,
379 and playing an important role in landslide initiation (Zhao et al., 2022; Cai et al., 2024; Chen et al., 2024; Lann et
380 al., 2024). In this context, our results highlight the hydro-mechanical heterogeneity across the *Robinia pseudoacacia*-
381 dominated woodland and *Rosa xanthina*-dominated shrubland, and assessed its influence on landslide initiation.

382 The results of SWCC and HCF agree well with the infiltration patterns observed in dye-tracer experiments. In
383 woodland soils, continuous preferential flow channels promote rapid infiltration, substantial downward water
384 migration, and a high capacity for water storage and drainage. Shrubland soils exhibit scattered preferential flow
385 channels, shorter infiltration pathways, pronounced shallow saturation, and a weaker capacity for water
386 redistribution. The stained area ratio and patch distribution further corroborate these differences. Woodland profiles
387 display vertical and continuous stained bands with greater infiltration depths, whereas shrubland profiles show
388 shallow staining. This comparison indicates that variations in root distribution and diameter modify soil pore
389 structure and thereby affect infiltration (Guan et al., 2024; Lann et al., 2024). Woodland soil with coarse roots and
390 higher porosity facilitate deeper infiltration, whereas shrubland soils with shallow root systems provide lower
391 infiltration capacity (Souza et al., 2023; Xiao et al., 2024; Hu et al., 2025). Preferential flow may result in the excess
392 soil water storage over the rainfall depth, and the results from monitoring multiple natural rainfall events between
393 20 May and 6 July 2023 further corroborate the assumption. In shrubland, soil moisture typically exhibits a delayed
394 and attenuated response to rainfall. R_c values are consistently below zero, indicating low rainfall conversion
395 efficiency. Most rainwater does not infiltrate but instead runs off once shallow soils saturate rapidly. In contrast,
396 once rainfall over woodland slopes reaches a certain intensity, R_c values become positive. This pattern suggests that
397 woodland slopes effectively intercept and infiltrate rainfall, sustain deeper water storage, and delay the development
398 of saturation zones. This discrepancy is also evident in the critical $a_{eq} \times R_t$ values. The failure resistance on woodland
399 slopes is higher than shrubland slopes, which may explain the contrasting distribution patterns observed in landslide
400 number and size.

401 Vegetation-based slope protection has long been regarded as a key measure in traditional soil and water
402 conservation, yet multidisciplinary studies have revealed its dual effects (Gyssels et al., 2005; Sidle and Bogaard,
403 2016; Lann et al., 2024). Some herbaceous plants with shallow root systems can promote rapid surface saturation
404 during intense rainfall, thereby enhancing hillslope runoff and rill erosion (Gong et al., 2024). Certain fast-growing
405 tree species with shallow root systems may provide only limited soil reinforcement and thus increase the risk of
406 shallow landslides (Ghestem and Sidle, 2011; Lin et al., 2024). Moreover, excessively thick litter layers can impede
407 infiltration during short-duration storms and accelerate runoff concentration (Zhou et al., 2018; Rajão et al., 2023).
408 These observations indicate that vegetation-based measures are not universally effective for soil erosion control
409 (Löbmann et al., 2020; Lann et al., 2024). Our results further support this understanding. Shallow landslide initiation
410 depends not only on rainfall but also on vegetation type, which modifies coupled hydrological-mechanical processes
411 on slopes. The deep root systems and stable preferential flow channels in woodland slopes may provide greater
412 resilience against slope failure compared to shrubland slopes. This finding provides empirical evidence for forest-
413 type allocation in ecologically sensitive areas. It also highlights the need for appropriate vegetation-type selection
414 and matching in regional soil and water conservation.

删除了: -

删除了: -

删除了: $a_{cr} \times R_t$

设置了格式: 非上标/下标

418 **6 Conclusions**

419 Vegetation recovery on the Chinese Loess Plateau has altered the dominant soil erosion process from runoff-
420 driven erosion to gravity-driven mass movements. Though previous studies have extensively investigated vegetation
421 effects on soil erosion, the specific role of vegetation in landslide initiation remains poorly understood. In this study,
422 we systematically examined landslide initiation processes in two contrasting vegetated landscapes: *Robinia*
423 *pseudoacacia*-dominated woodlands and *Rosa xanthina*-dominated shrublands, focusing on hydro-mechanical
424 heterogeneity. Following results can be drawn:

425 1. Landslides in woodland and shrubland exhibit obvious differences in initiation, depth and number. Shrubland
426 has a higher density of small, shallow landslides, whereas woodland has fewer but deeper and larger failures. This
427 contrast reflects a high-initiation-threshold and deep-seated-failure regime in woodland.

428 2. In shrubland, a loose, discontinuous pore system and pronounced hysteresis concentrate moisture in shallow
429 layers, causing rapid shallow saturation and large rainfall losses. In woodland, stable preferential flow paths promote
430 deeper and more efficient moisture migration, as reflected in higher soil water response index.

431 3. Woodland roots extend deeper and span a wider depth range than shrubland roots. Within the same depth
432 interval, root additional cohesion and *RAR* are also higher than those in shrubland. These patterns indicate stronger
433 root-network reinforcement in woodland soils and lower susceptibility to shallow landslides than in shrubland.
434 Therefore, the sediment production from landslide erosion may differ in various forest types, which has been rarely
435 addressed and deserves further study in future.

436 **Acknowledgments**

437 This research has been supported by the State Key Program of Natural Science of China (grant no. 42130701), and
438 the Natural Science Foundation of China (grant no. 42177309). The authors extend their gratitude to personnel at
439 the Jixian National Ecosystem Research Station of Shanxi Province, Beijing Forestry University, for their help during
440 field investigations.

441 **Code and data availability**

442 The corresponding author, Prof. Chao Ma, is willing to share the raw/processed data upon reasonable request.

443 **Author contributions**

444 **Prof. Ma** conceived the study based on his expertise in shallow landslides and unsaturated soil mechanics, and
445 proposed the concept of hydrological and hydromechanical coupling for analyzing vegetation-related slope
446 instability. Under the guidance of Prof. Ma, **Ruijie Yang** conducted soil hydrology experiments and drafted the
447 manuscript. **Xi Yang and Xinying Wang** assisted with field investigations. **Yan Zang and Liqun Lyu** contributed
448 research progress on shallow landslides and vegetation–slope interactions in the study area.

449 **Competing interests**

450 The authors declare no conflicts of interest.

451 **References**

452 An, J., Gao, G., Yuan, C., and Fu, B.: Inter- and intra-event rainfall partitioning dynamics of two typical xerophytic
453 shrubs in the loess plateau of china, *Hydrology and Earth System Sciences Discussions*, 26, 3885-3900,
454 <https://doi.org/10.5194/hess-26-3885-2022>, 2022.
455 Bachmair, S., Weiler, M., and Troch, P. A.: Intercomparing hillslope hydrological dynamics: spatio-temporal

删除了: -

删除了: -

458 variability and vegetation cover effects, *Water Resour. Res.*, 48, W5537, <https://doi.org/10.1029/2011WR011196>,
459 2012.

460 Bai, R., Wang, X., Li, J., Yang, F., Shangguan, Z., and Deng, L.: The impact of vegetation reconstruction on soil
461 erosion in the loess plateau, *J. Environ. Manage.*, 363, 121382, <https://doi.org/10.1016/j.jenvman.2024.121382>,
462 2024.

463 Borrelli, P., Robinson, D. A., Panagos, P., Lugato, E., Yang, J. E., Alewell, C., Wuepper, D., Montanarella, L., and
464 Ballabio, C.: Land use and climate change impacts on global soil erosion by water (2015-2070), *Proc. Natl. Acad.*
465 *Sci. U. S. A.*, 117, 21994-22001, <https://doi.org/10.1073/pnas.2001403117>, 2020.

466 Cai, L., Wang, F., Lin, Y., Long, Q., Zhao, Y., Han, J., Ge, W., and Chen, H.: Changes in preferential flow caused
467 by root effects in black locust plantations of different stand ages in the semi-arid region of the loess plateau, *J.*
468 *Hydrol.*, 634, 131086, <https://doi.org/10.1016/j.jhydrol.2024.131086>, 2024.

469 Chen, M., Yang, X., Zhang, X., Bai, Y., Shao, M., Wei, X., Jia, Y., Wang, Y., Jia, X., Zhu, Y., Zhang, Q., Zhu, X.,
470 and Li, T.: Response of soil water to long-term revegetation, topography, and precipitation on the chinese loess
471 plateau, *Catena*, 236, 107711, <https://doi.org/10.1016/j.catena.2023.107711>, 2024.

472 Deng, J., Ma, C., and Zhang, Y.: Shallow landslide characteristics and its response to vegetation by example of july
473 2013, extreme rainstorm, central loess plateau, china, *Bull. Eng. Geol. Environ.*, 81, 100, <https://doi.org/10.1007/s10064-022-02606-1>, 2022.

475 Dibiagio, A., Capobianco, V., Oen, A., and Tallaksen, L. M.: State-of-the-art: parametrization of hydrological and
476 mechanical reinforcement effects of vegetation in slope stability models for shallow landslides, *Landslides*, 21,
477 2417-2446, <https://doi.org/10.1007/s10346-024-02300-1>, 2024.

478 Du, P., Chen, Y., Zhao, Y., Qu, L., Liu, H., Liu, Z., Xu, J., and Tian, X.: Formation process and depositional
479 characteristics of mudballs in the loess plateau during extreme rainstorms: dual-threshold constraints on material
480 sources and dynamic conditions, *J. Environ. Manage.*, 391, 126590, [https://doi.org/10.1016/j.jenvman.2025.](https://doi.org/10.1016/j.jenvman.2025.126590)
481 126590, 2025.

482 Fan, L., Lehmann, P., Zheng, C., and Or, D.: Rainfall intensity temporal patterns affect shallow landslide triggering
483 and hazard evolution, *Geophys. Res. Lett.*, 47, e2019GL085994, [https://doi.org/https://doi.org/10.1029/2019GL](https://doi.org/https://doi.org/10.1029/2019GL085994)
484 085994, 2020.

485 Feng, X., Fu, B., Piao, S., Wang, S., Ciais, P., Zeng, Z., Lü, Y., Zeng, Y., Li, Y., Jiang, X., and Wu, B.: Revegetation
486 in china's loess plateau is approaching sustainable water resource limits, *Nat. Clim. Chang.*, 6, 1019-1022,
487 <https://doi.org/10.1038/nclimate3092>, 2016.

488 Franklin, S. M., Kravchenko, A. N., Vargas, R., Vasilas, B., Fuhrmann, J. J., and Jin, Y.: The unexplored role of
489 preferential flow in soil carbon dynamics, *Soil Biology and Biochemistry*, 161, 108398, [https://doi.org/10.1016/](https://doi.org/10.1016/j.soilbio.2021.108398)
490 [j.soilbio.2021.108398](https://doi.org/10.1016/j.soilbio.2021.108398), 2021.

491 Fu, B., Wang, S., Liu, Y., Liu, J., Liang, W., and Miao, C.: Hydrogeomorphic ecosystem responses to natural and
492 anthropogenic changes in the loess plateau of china, *Annual Review of Earth & Planetary Sciences*, 45, 223-243,
493 <https://doi.org/10.1146/annurev-earth-063016-020552>, 2016.

494 Ghestem, M. and Sidle, R.: The influence of plant root systems on subsurface flow: implications for slope stability,
495 *Bioscience*, 61, 869-879, <https://doi.org/10.1525/bio.2011.61.11.6>, 2011.

496 Gong, C., Ni, D., Liu, Y., Li, Y., Huang, Q., Tian, Y., and Zhang, H.: Herbaceous vegetation in slope stabilization:
497 a comparative review of mechanisms, advantages, and practical applications, *Sustainability*, 16, 7620,
498 <https://doi.org/10.3390/su16177620>, 2024.

499 Gu, C., Mu, X., Gao, P., Zhao, G., Sun, W., Tatarko, J., and Tan, X.: Influence of vegetation restoration on soil
500 physical properties in the loess plateau, china, *J. Soils Sediments*, 19, 716-728, <https://doi.org/10.1007/s11368->

018-2083-3, 2019.

502 Guan, N., Bi, H., Song, Y., Lu, S., Lin, D., and Han, J.: Vegetation restoration is affecting the characteristics and
503 patterns of infiltration in the loess plateau, *Catena*, 243, 108190, <https://doi.org/10.1016/j.catena.2024.108190>,
504 2024.

505 Gyssels, G., Poesen, J., Bochet, E., and Li, Y.: Impact of plant roots on the resistance of soils to erosion by water: a
506 review, *Progress in Physical Geography*, 29, 189-217, <https://doi.org/10.1191/0309133305pp443ra>, 2005.

507 Hao, M., Jin, Z., Luo, D., Cao, G., Jiang, C., Han, H., Yang, S., and Zhang, J.: Rainstorm erosion difference and
508 topographical changes induced by heavy rainfall between afforestation and grassland restoration catchments on
509 the chinese loess plateau, *Geomorphology*, 457, 109243, <https://doi.org/10.1016/j.geomorph.2024.109243>, 2024.

510 Hu, J., Ren, Y., Tang, M., Zhang, Z., Yang, K., Zhen, Q., and Han, F.: Effects of vegetation restoration on infiltration
511 patterns and preferential flow in semi-arid areas with shallowly buried soft bedrock (pisha sandstone) in china, *J.*
512 *Hydrol.*, 661, 133546, <https://doi.org/10.1016/j.jhydrol.2025.133546>, 2025.

513 Lan, H., Zhao, X., Macciotta, R., Peng, J., Li, L., Wu, Y., Zhu, Y., Liu, X., Zhang, N., and Liu, S.: The cyclic
514 expansion and contraction characteristics of a loess slope and implications for slope stability., *Sci. Rep.*, 11, 2250,
515 <https://doi.org/10.1038/s41598-021-81821-4>, 2021.

516 Lann, T., Bao, H., Lan, H., Zheng, H., Yan, C., and Peng, J.: Hydro-mechanical effects of vegetation on slope
517 stability: a review, *Sci. Total Environ.*, 926, 171691, <https://doi.org/10.1016/j.scitotenv.2024.171691>, 2024.

518 Laycock, W. A., Geological Survey U. S., I. B., New, J. D. O. W., United, S. F. S., and Rutgers, U. (Eds.):
519 Distribution of roots and rhizomes in different soil types in the pine barrens of new jersey, U.S. Geological Survey
520 Professional Paper, Washington, 1967.

521 Li, F., Song, X., Tang, C., Liu, C., Yu, J., and Zhang, W.: Tracing infiltration and recharge using stable isotope in
522 taihang mt., North china, *Environmental Geology*, 53, 687-696, <https://doi.org/10.1007/s00254-007-0683-0>, 2007.

523 Li, J., Cui, P., and Yin, Y.: Field observation and micro-mechanism of roots-induced preferential flow by infiltration
524 experiment and phase-field method, *J. Hydrol.*, 623, 129756, <https://doi.org/10.1016/j.jhydrol.2023.129756>, 2023.

525 Li, S., Zheng, C., Lu, T., Zhou, K., Gu, Y., Wang, B., and Lu, Y.: Characteristics and influencing factors of loess
526 terraces' preferential flow under different typical vegetation cover, *Plant Soil*, in press, <https://doi.org/10.1007/s11104-025-07710-1>, 2025.

528 Liang, H., Li, Y., An, X., Liu, J., Pan, N., and Li, Z.: Soil moisture dynamics and its temporal stability under
529 different-aged caragana korshinskii shrubs in the loess hilly region of china, *Water*, 15, 2334, <https://doi.org/10.3390/w15132334>, 2023.

531 Liao, J., Wang, J., Jiao, J., Yan, Z., Li, J., Zhang, Z., Li, M., Xu, Q., Jiang, X., Zhao, W., Ling, Q., Sheng, H., Chen,
532 Y., and Wu, T.: Rusle tends to overestimate soil erosion in revegetated conditions: evidence from long-term runoff
533 plots monitoring on china's loess plateau, *Catena*, 258, 109285, <https://doi.org/10.1016/j.catena.2025.109285>,
534 2025.

535 Lin, Y., Jian, W., Wu, Y., Zhu, Z., Wang, H., Dou, H., and Lai, Z.: Effect of tree roots on heavy rainfall-induced
536 shallow landslides, *Geomatics, Natural Hazards and Risk*, 15, 2360002, <https://doi.org/10.1080/19475705.2024.2360002>, 2024.

538 Liu, X., Feng, T., Zhang, Y., Liu, Y., and Wang, P.: Vegetation restoration affects soil hydrological processes in
539 typical natural and planted forests on the loess plateau, *J. Hydrol.*, 650, 132465, <https://doi.org/10.1016/j.jhydrol.2024.132465>, 2025.

541 Löbmann, M. T., Geitner, C., Wellstein, C., and Zerbe, S.: The influence of herbaceous vegetation on slope stability
542 – a review, *Earth-Sci. Rev.*, 209, 103328, <https://doi.org/10.1016/j.earscirev.2020.103328>, 2020.

543 Lu, N. and Godt, J. W. (Eds.): Hillslope hydrology and stability, Cambridge University Press, Cambridge, U.K.,

删除了: Li, P., Pan, Z., Xiao, T., and Wang, J.: Effects of molding water content and compaction degree on the microstructure and permeability of compacted loess, *Acta Geotech.*, 18, 921-936, <https://doi.org/10.1007/s11440-022-01592-8>, 2023.

549 2013.

550 Lu, N., Calderon, A. R. A., Wayllace, A., Lovekin, J., and Crandall, A.: Suction stress-based rainfall intensity–
551 duration method for slope instability prediction, *J. Geotech. Geoenviron. Eng.*, 150, 4024069, [https://doi.org/](https://doi.org/10.1061/JGGEFK.GTENG-12597)
552 10.1061/JGGEFK.GTENG-12597, 2024.

553 Masi, E. B., Tofani, V., Rossi, G., Cuomo, S., Wu, W., Salciarini, D., Caporali, E., and Catani, F.: Effects of roots
554 cohesion on regional distributed slope stability modelling, *Catena*, 222, 106853, [https://doi.org/10.1016/j.catena.](https://doi.org/10.1016/j.catena.2022.106853)
555 2022.106853, 2023.

556 Montgomery, D. R. and Dietrich, W. E.: A physically based model for the topographic control on shallow landsliding,
557 *Water Resour. Res.*, 30, 1153-1171, <https://doi.org/10.1029/93WR02979>, 1994.

558 Montgomery, D. R. and Dietrich, W. E.: Landscape dissection and drainage area-slope thresholds, in: *Process*
559 *Models and Theoretical Geomorphology*, edited, John Wiley & Sons, Chichester, 221-246, 1994.

560 Montgomery, D. R., Schmidt, K. M., Greenberg, H. M., and Dietrich, W. E.: Forest clearing and regional landsliding,
561 *Geology*, 28, 311-314, [https://doi.org/10.1130/0091-7613\(2000\)28<311:FCARL>2.0.CO;2](https://doi.org/10.1130/0091-7613(2000)28<311:FCARL>2.0.CO;2), 2000.

562 Nimmo, J. R., Perkins, K. S., Schmidt, K. M., Miller, D. M., Stock, J. D., and Singha, K.: Hydrologic characterization
563 of desert soils with varying degrees of pedogenesis: 1. Field experiments evaluating plant-relevant soil water
564 behavior, *Vadose Zone J.*, 8, 480-495, <https://doi.org/10.2136/vzj2008.0052>, 2009.

565 Niu, F., Pan, C., and Cui, Y.: Experimental investigation to the effect of different land-use on rainfall infiltration
566 runoff patterns and preferential flow distribution in the loess area of western shanxi province, *Acta Ecologica*
567 *Sinica*, 43, 4144-4166, <https://doi.org/10.5846/stxb202204130989>, 2023.

568 Rajão, P., Berg, M., Cornelissen, J., and Dias, A.: The effects of leaf traits on litter rainfall interception with
569 consequences for runoff and soil conservation, *J. Ecol.*, 111, 2662-2675, <https://doi.org/10.1111/1365-2745.14203>,
570 2023.

571 Schwarz, M., Preti, F., Giadrossich, F., Lehmann, P., and Or, D.: Quantifying the role of vegetation in slope stability:
572 a case study in tuscany (italy), *Ecol. Eng.*, 36, 285-291, <https://doi.org/10.1016/j.ecoleng.2009.06.014>, 2010.

573 Sidle, R. C. and Bogaard, T. A.: Dynamic earth system and ecological controls of rainfall-initiated landslides, *Earth-*
574 *Sci. Rev.*, 159, 275-291, <https://doi.org/10.1016/j.earscirev.2016.05.013>, 2016.

575 Souza, L. F. T., Hirmas, D. R., Sullivan, P. L., Reuman, D. C., Kirk, M. F., Li, L., Ajami, H., Wen, H., Sarto, M. V.
576 M., Loecke, T. D., Rudick, A. K., Rice, C. W., and Billings, S. A.: Root distributions, precipitation, and soil
577 structure converge to govern soil organic carbon depth distributions, *Geoderma*, 437, 116569,
578 <https://doi.org/10.1016/j.geoderma.2023.116569>, 2023.

579 Tang, B., Jiao, J., Zhang, Y., Chen, Y., Wang, N., and Bai, L.: The magnitude of soil erosion on hillslopes with
580 different land use patterns under an extreme rainstorm on the northern loess plateau, china, *Soil and Tillage*
581 *Research*, 204, 104716, <https://doi.org/10.1016/j.still.2020.104716>, 2020.

582 Tang, P., Zhang, J., Li, Y., Wei, G., Hu, Y., and Zhao, J.: Effects of extreme rainfall on the morphological
583 characteristics and spatial distribution of shallow landslides under different land use patterns in the loess region of
584 western shanxi province, northern china, *Journal of Beijing Forestry University*, 45, 109-117, [https://doi.org/10.](https://doi.org/10.12171/j.1000-1522.20230070)
585 12171.j.1000-1522.20230070, 2023.

586 Wang, N. and Zhang, T.: Soil pore structure and its research methods: a review, *Soil Water Res.*, 19, 1-24,
587 <https://doi.org/10.17221/64/2023-SWR>, 2024.

588 Wang, R., Dong, Z., Zhou, Z., Wang, N., Xue, Z., and Cao, L.: Effect of vegetation patchiness on the subsurface
589 water distribution in abandoned farmland of the loess plateau, china, *Sci. Total Environ.*, 746, 141416,
590 <https://doi.org/10.1016/j.scitotenv.2020.141416>, 2020.

591 Wang, R., Dong, Z., Zhou, Z., and Wang, P.: Temporal variation in preferential water flow during natural vegetation

592 restoration on abandoned farmland in the loess plateau of china, *Land*, 8, 186, [https://doi.org/](https://doi.org/10.3390/land8120186)
593 10.3390/land8120186, 2019.

594 Wang, X., Ma, C., Lyu, L., and Zhang, Y.: Erosion characteristics of shallow landslides under various land-use
595 conditions: an example of the caijiachuan landslide, *Arid Zone Research*, 41, 697-705,
596 <https://doi.org/10.13866/j.azr.2024.04.15>, 2024.

597 Wang, Y., Dong, G., Qu, L., Wu, Z., Zhao, F., and Shao, C.: Ecosystem functioning of the loess plateau in china
598 from vegetation restoration relied largely on climate, *Forests*, 14, 27, <https://doi.org/10.3390/f14010027>, 2022.

599 Wei, Y. Z., Yao, Z. H., Chong, X. L., Zhang, J. H., and Zhang, J.: Microstructure of unsaturated loess and its
600 influence on strength characteristics, *Sci. Rep.*, 12, 1502, <https://doi.org/10.1038/s41598-022-05464-9>, 2022.

601 Wen, S., Shao, M., and Wang, J.: Earthworm burrowing activity and its effects on soil hydraulic properties under
602 different soil moisture conditions from the loess plateau, china, *Sustainability*, 12, 9303, [https://doi.org/](https://doi.org/10.3390/su12219303)
603 10.3390/su12219303, 2020.

604 Xiao, T., Li, P., Fei, W., and Wang, J.: Effects of vegetation roots on the structure and hydraulic properties of soils:
605 a perspective review, *Sci. Total Environ.*, 906, 167524, <https://doi.org/10.1016/j.scitotenv.2023.167524>, 2024.

606 Yamase, K., Ikeno, H., Hotta, N., Imawaka, M., Ohashi, M., Tanikawa, T., Todo, C., Dannoura, M., and Hirano, Y.:
607 Effect of sprouting and corresponding root distribution of the shrub species *Eurya japonica* on slope stability,
608 *Catena*, 238, 107869, <https://doi.org/10.1016/j.catena.2024.107869>, 2024.

609 Yan, X., Nunes, J. P., Sun, J., Tang, D., Wen, Y., and Li, Z.: Restored vegetation dominates the decrease in surface
610 and subsurface runoff on the loess plateau, *J. Hydrol.*, 640, 131730, <https://doi.org/10.1016/j.jhydrol.2024.131730>,
611 2024.

612 Yang, B., Jiao, J., Ma, X., Zhao, W., Ling, Q., Zhang, X., Han, J., Du, P., Chen, Y., and Chen, H.: Distribution and
613 formation of soil balls under heavy rainstorm conditions in the northern loess plateau, *J. Hydrol.*, 625, 130103,
614 <https://doi.org/10.1016/j.jhydrol.2023.130103>, 2023.

615 Yang, B., Ma, X., Jiao, J., Zhao, W., Ling, Q., Li, J., and Zhang, X.: Magnitude and hotspots of soil erosion types
616 during heavy rainstorm events on the loess plateau: implications for watershed management, *Catena*, 246, 108365,
617 <https://doi.org/10.1016/j.catena.2024.108365>, 2024.

618 Zhang, S., Liu, Y., Yang, M., Tian, P., Mu, X., and Zhao, G.: Impact of vegetation restoration on preferential flow
619 and soil infiltration capacity in the hilly region of the loess plateau, *Journal of Hydrology: Regional Studies*, 59,
620 102333, <https://doi.org/10.1016/j.ejrh.2025.102333>, 2025.

621 Zhang, Y., Tang, Z., Zhang, J., Zhang, Z., and Zhang, M.: Visualizing preferential flow paths using dye tracer and
622 species diversity theory methods to explore their correlation to soil properties with random forest algorithm, *J.*
623 *Hydrol.*, 638, 131570, <https://doi.org/10.1016/j.jhydrol.2024.131570>, 2024.

624 Zhao, M., Li, D., Huang, Y., Deng, Y., Yang, G., Lei, T., and Huang, Y.: Soil matrix infiltration characteristics in
625 differently aged eucalyptus plantations in a southern subtropical area in china, *Catena*, 217, 106490,
626 <https://doi.org/10.1016/j.catena.2022.106490>, 2022.

627 Zhou, Q., Zhou, X., Luo, Y., and Cai, M.: The effects of litter layer and topsoil on surface runoff during simulated
628 rainfall in guizhou province, china: a plot scale case study, *Water*, 10, 915, <https://doi.org/10.3390/w10070915>,
629 2018.

630

删除了: Xu, P., Zhang, Q., Qian, H., Li, M., and Yang, F.:
An investigation into the relationship between saturated
permeability and microstructure of remolded loess: a case
study from chinese loess plateau, *Geoderma*, 382, 114774,
<https://doi.org/10.1016/j.geoderma.2020.114774>, 2021.